Holocene glacier and ice cap fluctuations in southwest Greenland inferred from two lake records

Laura J. Larocca[a], Yarrow Axford[a], Sarah A. Woodroffe[b], G. Everett Lasher[a,c], & Barbara Gawin[a]

[a]*Department of Earth and Planetary Sciences, Northwestern University, 2145 Sheridan Road, Evanston, IL 60208 USA*

[b]*Department of Geography, Durham University, Lower Mountjoy South Rd, Durham, DH1 3LE, UK*

[c]*Department of Geology and Environmental Science, University of Pittsburgh, 4107 O'Hara Street, Pittsburgh, PA 15260 USA*

Keywords: Greenland, lake sediments, Holocene, paleoclimate, glaciers and ice caps, equilibrium-line altitudes, isolation basins

Abstract

Glaciers and ice caps (GICs) respond rapidly to changes in temperature and precipitation. Thus, records of their past fluctuations yield valuable information on past climate. However, relatively little is known about the long-term, Holocene history of Greenland's local GICs, peripheral to the Greenland Ice Sheet. Here we report sediment records of Holocene glacier activity from two distally fed glacial lakes near Buksefjord, southwest Greenland. The two lakes' watersheds host modern GICs of contrasting size. The Pers Lake (informal name) watershed drains part (3 km^2) of a single small ice cap. In contrast, nearby Lake T3's (informal name) watershed drains numerous GICs totaling 100 km^2. At the time it emerged from the sea ~8.6 ka BP, Pers Lake was receiving no glacial meltwater input. Sediment physical and geochemical properties indicate persistent meltwater input and regrowth of the ice cap within the Pers Lake catchment beginning at ~1.4 ka BP, after almost 3000 years of sporadic meltwater input beginning ~4.3 ka BP. The ice cap above Pers Lake reached a maximum late Holocene extent during the final phase of the Little Ice Age (LIA), ~0.1 ka BP. The complementary Lake T3 sediment record suggests continued meltwater input from the larger suite of upstream GICs from the time of the lake's isolation from the sea ~8.4-7.5 ka BP through to the present. This indicates that some GICs here probably survived the Holocene Thermal Maximum (HTM), although were significantly reduced in size for an extended period (of unknown age and duration). Combined with evidence from Pers Lake and prior studies that show GICs at low and intermediate elevations in this region melted away completely during the HTM, and evidence for GIC presence at Lake T3, we provide lower and upper bounds on regional HTM ELAs. We estimate that regional equilibrium-line altitudes (ELAs) were between ~1370 and 1470 meters above sea level in the early-to-middle Holocene. From the middle to late Holocene, our results, along with other regional GIC studies, indicate progressive lowering of regional glacier ELAs in response to Neoglacial summer cooling of ~2.7ºC, assuming no change in precipitation.

1. Introduction

Over the past century, local glaciers and ice caps (GICs) peripheral to the Greenland ice sheet (GrIS) have responded rapidly, on a decadal scale, to changes in climate (Bjørk et al., 2012; Leclercq et al., 2012), and are especially sensitive to changes in summer temperature (Oerlemans, 2001; 2005). In recent decades, anthropogenic warming has caused most of Greenland's ~20,300 GICs to retreat, with future mass losses estimated to be at least 2016 ± 129 Gt to 3907 ± 108 Gt by 2098 C.E. (Rastner et al., 2012; Machguth et al., 2013). While modern-day observations are essential for refining our understanding of the mechanisms that control glacier mass balance, knowledge of past GIC fluctuations is important to place recent changes into a longer-term perspective. Moreover, additional Holocene records of GIC variability will place better constraints on their sensitivity to sustained periods of warmer than present conditions and will help to clarify regional Holocene climate trends. Yet, beyond the short-term historical record, current knowledge of the longer-term Holocene history of Greenland's outlying GICs is still very sparse.

In Greenland, much of the evidence of past GIC activity is fragmentary because recent local glacier advances have destroyed much of the geomorphic evidence of glacier extents from earlier in the Holocene. Most local glaciers reached a historical maximum (which most typically was their most extensive position since at least the early Holocene) during the Little Ice Age (LIA; 1250-1900 C.E.) (Kelly and Lowell, 2009). However, lake sediment records have been effectively used to reconstruct full-Holocene, high-resolution records of local GIC activity in Greenland (e.g, Möller et al., 2010; Lowell et al., 2013; Levy et al., 2014; Balascio et al., 2015; Larsen et al., 2017; Schweinberg et al., 2017; Schweinberg et al., 2018; van der Bilt et al., 2018; Larsen et al., 2019; Axford et al., 2019; Larocca et al., 2020), and have provided valuable insights into the spatial and temporal variability in Holocene climate. Although the number of studies that capture continuous records of GIC fluctuations across Greenland is still small, they show that most GICs fluctuated significantly through the Holocene in response to millennial scale climate changes driven by changes in Northern Hemisphere summer insolation, and likely in response to other regional, sub-millennial scale forcings, such as changes in ocean circulation, episodic meltwater releases, and volcanism (Balascio et al., 2015; Schweinberg et al., 2017; Schweinberg et al., 2019).

In general, most GICs were smaller than present or completely absent in the warm early-to-middle Holocene, and subsequently expanded or regrew as temperatures cooled in the late Holocene (Briner et al., 2016; Larsen et al., 2019). In addition, a recent compilation of continuous Holocene GIC records from Greenland suggests that glacier response to warmer than present conditions during the Holocene thermal maximum (HTM) is correlated to both latitude and elevation: in the southern half of Greenland, most records show that GICs melted away completely during the HTM (except for the high elevation Renland Ice Cap), while some records from the north show that GICs became smaller than present but survived the HTM (Larsen et al., 2019). It has also been suggested that the timing of GIC disappearance or reduction in extent is associated with latitude, and thus, the onset of the regional HTM—with GICs in south Greenland becoming smaller or melting away later in the Holocene than those in the north (Larocca et al., 2020). This supports other arctic paleoclimate reviews that suggest a delayed HTM in southern Greenland, and an overall complex climatic response to insolation and other forcings through the Holocene around the northern North Atlantic (Kaufman et al., 2004; Briner et al., 2016).

In southwest Greenland, there are only two studies that provide continuous records of Holocene local GIC fluctuations (e.g., Fig. 1B; Larsen et al., 2017; Schweinsberg et al., 2018). Moreover, terrestrial paleotemperature records from beyond the GrIS in the Nuuk region, and in other proximate areas of southwest Greenland, near Kangerlussuaq and Sisimiut (Fig. 1B), are limited (e.g., Fredskild, 1983; Aebly and Fritz, 2009; Bennike et al., 2010; D'Andrea et al., 2011;

Perren et al., 2012; Wagner and Bennike, 2012; Law et al., 2015; Lasher et al., 2020). To date, there is no strong consensus on the timing or magnitude of peak HTM warmth in southwest Greenland (between Nuuk and Kangerlussuaq), although most studies suggest generally warm conditions between ~9 and 5 ka BP.

Here, we investigate local GIC variability in southwest Greenland by evaluating the geochemical and physical properties of lake sediments. We present sediment records from two distally fed glacial lakes, Pers Lake and Lake T3 located south of Nuuk (Fig. 1C). We compare our results with other published local glacier records from the region and place constraints on regional glacier equilibrium-line altitudes (ELAs) during the Holocene.

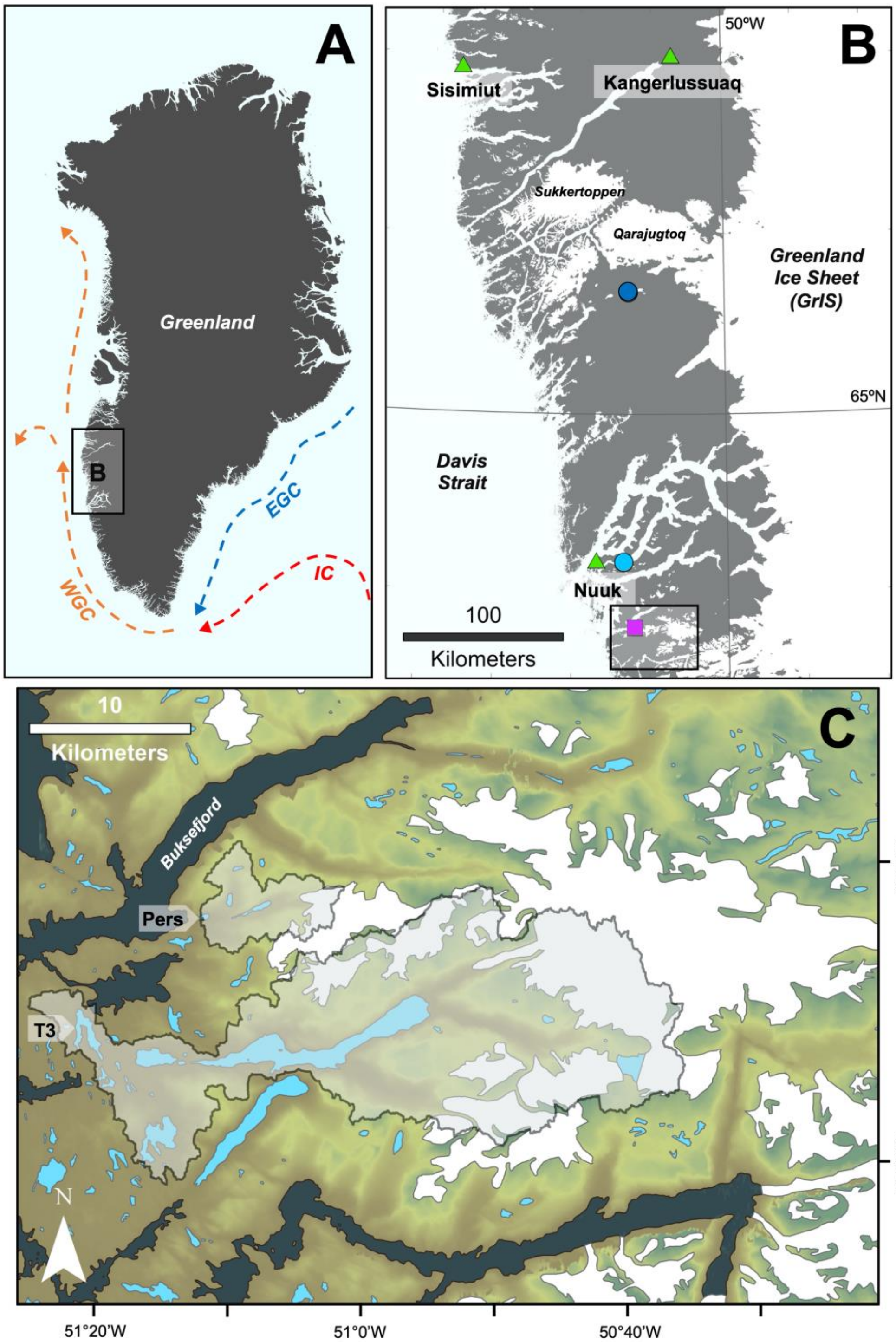

Figure 1. Location of the study area within Greenland. **A.** Major ocean currents. WGC is the West Greenland Current (orange), EGC is the East Greenland Current (blue), and IC is the Irminger Current (red) (Dietrich et al., 1980). **B.** Southwest Greenland including locations discussed in the

text (green triangles), published regional records of GIC fluctuations (light blue circle is Larsen et al., 2017; dark blue circle is Schweinsberg et al., 2018), and our study area (purple square). Land is shown in gray, and ice in white. **C.** Locations of Pers Lake and Lake T3 in the Buksefjord region. Local GICs are shown in white and the lake watersheds are in shaded polygons.

2. Geographical Setting, Climate, and Glaciation History

The fjord lined coast of southwest Greenland neighbors the Davis Strait, the northern boundary of the Labrador basin (Fig. 1B). The present-day inland ice margin of the GrIS is located ~100-170 km to the east of the coast. The West Greenland current (WGC) flows northward along the coast and integrates relatively warm and saline Atlantic water from the Irminger current (IC), with cold, low salinity water from the East Greenland current (EGC) (Fig. 1A). Our study area is located ~50 km south of Nuuk, near Buksefjord (Fig. 1B and C) in a region of areally-scoured uplands with relatively shallow and narrow fjords (Larsen et al., 2014). Presently the southwest region hosts ~1300 local GICs, that cover ~6500 km^2 in total area. The GICs have an average minimum and maximum elevation of ~780 and ~1210 meters above sea level (m a.s.l.) respectively (Raup et al., 2007). Most of the region's GICs are clustered around the Sukkertoppen region and south of Nuuk, with the low-relief land in between sparsely glaciated. The largest local GICs in the region are the Qarajugtoq and Sukkertoppen ice caps, both ~2000 km^2 in area (Fig. 1B) (Kelly and Lowell, 2009).

The modern climate of the Nuuk region is low arctic. In Nuuk, mean annual air temperature is –1.4°C, mean summer (JJA; June, July, August) air temperature is 5.8°C, and annual precipitation is 781.6 mm (1981-2010) (Cappelen, 2018). In some areas, a large climatic gradient exists between the coast and inland areas (Fredskild, 1983). The bedrock of the study area is Archean orthogneiss that is granodioritic to tonalitic in composition (GEUS, 2018) and vegetation is primarily dwarf shrub tundra.

During the Last Glacial Maximum (LGM, 26-19 ka BP; Clark et al., 2009), the southwestern GrIS extended onto the continental shelf. A marine sediment record from the southeastern Davis Strait suggests that retreat from the shelf break began before ~18.6 ka BP, and that the ice margin reached the middle to inner shelf between ~16.7-11 ka BP (Winsor et al., 2015). Mean cosmogenic ^{10}Be exposure ages on paired bedrock and boulder samples along a transect near Buksefjord suggest rapid ice sheet retreat in the early Holocene (between 10.7 ± 0.6 and 10.1 ± 0.4 ka BP) from the outer coast to the present-day ice margin (Fig. 2A) (Larsen et al., 2014).

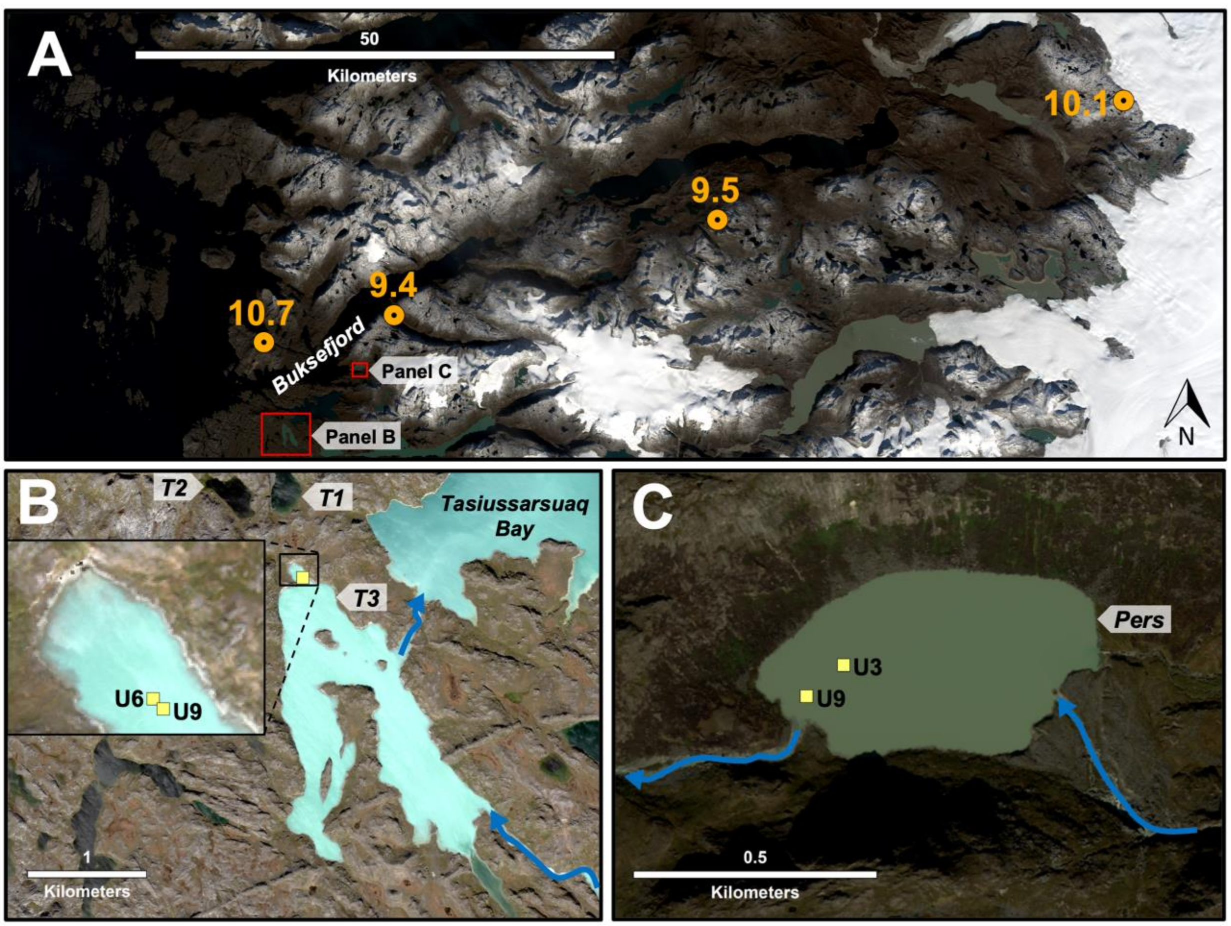

Figure 2. Major features of the study area **A.** Deglaciation ages in ka (thousands of years before present) from cosmogenic ^{10}Be exposure dating are in orange (Larsen et al., 2014). Our study lakes are in red boxes—Lake T3 is on the left (panel B) and Pers Lake is on the right (panel C) (September 21, 2016 Landsat-8 image from U.S. Geological Survey). **B.** Lake T3 with sediment core sites in yellow squares. Locations of nearby non-glacial lakes (T1 and T2) also cored in 2015 are shown north of Lake T3 (Lasher et al., 2020). Solid blue arrows show main inflow and outflow into Tasiussarsuaq Bay, connected to Buksefjord. **C.** Pers Lake with locations of sediment cores in yellow squares. Solid blue arrows show inflow and outflow into Buksefjord (September 8, 2010 Worldview-2 imagery copyright 2020 Digital Globe, Inc.).

3. Methods

3.1. Study sites and field methods

Sediment cores from two distally fed glacial lakes adjacent to Buksefjord were collected in August 2015 (Fig. 2B and C). Cores were obtained using a piston-free Universal check-valve percussion corer and all investigated cores were recovered with an intact sediment-water interface. Two lakes with contrasting catchment sizes and upstream GIC characteristics were targeted to place constraints on regional ELAs during the Holocene.

Pers Lake is a small (~0.2 km^2, ~25 m maximum depth) lake, situated at 20 m a.s.l. and thus below the local marine limit (which is estimated to be between 110 and 80 m a.s.l. near Nuuk in the early Holocene) (Long et al., 2011; Lecavalier et al., 2014). Meltwater from a ~20 km^2 ice cap to the east, which is partially inside the lake's 33 km^2 catchment, flows a total of ~6 km and through two upstream glacial lakes before reaching Pers Lake. At present, approximately 3 km^2 of the ice cap is located within the lake's catchment, and that ice has an elevation range of 479-975 m a.s.l. Today, the ice cap's highest point is at ~1275 m a.s.l. Two sediment cores were investigated. 15-PLK-U3 (N 63.8032, W 51.19869) is a 209 cm core retrieved at 18.2 m water depth and 15-PLK-U9 (N 63.80261, W 51.20021) is 180 cm long and was recovered at 6.1 m water depth (Fig. 2C).

Lake T3 is ~10 km southwest of Pers Lake, is relatively large (~2.0 km^2, unknown maximum depth), is situated at 7 m a.s.l., and has a large catchment area of ~350 km^2. At present meltwater from several large GICs flows up to ~25 km through three upstream glacial lakes before reaching T3. Approximately 100 km^2 of ice is located within the lake's catchment, comprising numerous small mountain glaciers and ice caps with surfaces between 447-1467 m a.s.l. Two sediment cores were investigated. 15-T3-U9 (N 63.751654, W 51.352970) is a 151 cm core retrieved at 8.8 m water depth and 15-T3-U6 (N 63.751697, W 51.353074) is 96 cm long and was recovered at 8.5 m water depth. Both cores were recovered from a small sub-basin on the north end of the lake (Fig. 2B).

3.2. Sediment characterization

In glacial lakes where the primary source of minerogenic material transported into the lake is provided by glacial erosion, there is a robust relationship between lake sediment properties and glacier activity (e.g., Nesje et al., 2000; Dahl et al., 2003; Balascio et al., 2015). Given that the soil cover in our study area is thin (0-30 cm), and that most of the slopes surrounding both lake sites are shallow (limiting mass wasting events), we interpret changes in minerogenic input as reflective of changes in upstream GIC size. We note that an exception to this is the steeper northern slope at Pers Lake. Since the GICs are not completely located inside the lake catchments, we consider our records as on-off threshold-style records (Dahl et al., 2003). We interpret inorganic sediment dominated by fine grained silty-clay as indicative of the presence of GICs inside the lake's catchment, and alternatively sediment higher in organic material (gyttja) as indicative of GICs reduced in size, beyond the boundary of the lake's catchment. In some cases, this configuration allows for an approximate location of the glacier terminus and an ELA constraint to be established when the ice is at or near this threshold (Dahl et al., 2003).

To characterize the sediment as glacially or non-glacially derived, we measured magnetic susceptibility (MS), visible color reflectance, and major element abundance on a Geotek multi-sensor core logger (MSCL-S) at 2 mm resolution. The Geotek MSCL-S is equipped with a Bartington point sensor (MS2E), a Konica Minola CM-700d spectrophotometer, and an Olympus DELTA Professional X-Ray Florescence (XRF) spectrometer that is configured with a 40kV Rhodium anode X-ray tube. XRF measurements were made with a dwell time of 30 seconds with the core surface covered in a 4μm Ultralene film. Sediment organic matter content was determined by loss-on-ignition (LOI) by combustion of dried 1-cm^3 bulk sediment samples at 550°C for 4 hours (e.g., Heiri et al., 2001). LOI was analyzed at 2 cm intervals on both Pers lake cores, at 2 cm intervals from 0-56 cm and at 10 cm intervals from 56-86 cm on T3 lake core U6, and at 2 cm intervals from 0-70 cm and at 10 cm intervals from 70-150 on T3 lake core U9. Percent carbon and nitrogen (%C, %N) and their isotope values ($\delta^{13}C$, $\delta^{15}N$) were measured on twenty-six bulk sediment samples from the Lake T3 cores using a Costech 4010 Elemental Analyzer (EA) coupled to a Thermo Scientific Delta V-Plus Isotope Ratio Mass Spectrometer (IRMS) at Northwestern's Integrated Laboratories for Earth and Planetary Sciences. Samples were not acidified prior to analysis.

3.3. Chronology

Core chronologies were established through radiocarbon dating of terrestrial plant fragments (n = 4, from lacustrine sediments) and mollusks (n = 3, from basal marine sediments) where available (Table 1). AMS ^{14}C ages were determined at Woods Hole Oceanographic Institution's National Ocean Sciences Accelerator Mass Spectrometry Facility (NOSAMS). The ^{14}C ages on the plant material were calibrated using CALIB version 7.1 and the IntCal13 calibration curve, and the marine samples (mollusks) were calibrated using the Marine13 curve (Reimer et al., 2013). We apply a ΔR of 115 ± 103 to the marine samples, the average of the 10 nearest samples, excluding deposit feeder species, from the Marine Reservoir Database (Reimer and Reimer, 2001). Calibrated ages are reported as the midpoint of the 2σ range, ± half of the 2σ range. No plant remains or other organic material large enough for radiocarbon dating could be found in the lacustrine sections of the Lake T3 cores, or in the U9 Pers Lake core. As described in the Discussion, we used comparisons with nearby ^{14}C-dated lakes to estimate the timing of marine isolation (i.e., the onset of lacustrine sedimentation) for Lake T3 and Pers Lake. An age-depth model was generated for core PLK-U3 using the Bacon age modeling package in R, version 2.2 (Blaauw and Christen, 2011), and the median was used for data interpretation (Fig. 3). Three radiocarbon dates from the U3 core and the best estimate of isolation of Pers Lake (from 15-T1-U4, i.e. ~8.6 ka BP) were included in the model input (see Discussion). The top of the core was set to the year of collection, AD 2015 (–65 cal yr BP).

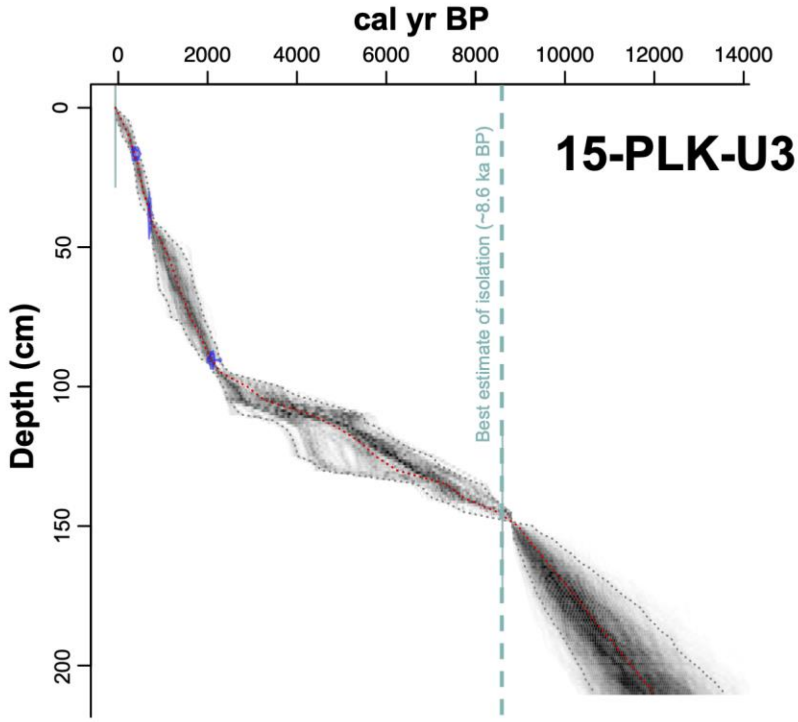

Figure 3. Age-depth model for core PLK-U3 generated using the Bacon age modeling package in R, version 2.2 (Blaauw and Christen, 2011). Calibrated ^{14}C dates and their probability density functions are in blue. Darker greys indicate more likely calendar ages bounded by 95% confidence intervals (dotted gray lines). The red dotted line shows the 'best' model based on the weighted mean age for each depth. The cyan dotted line shows the best estimate of isolation, ~8.6 ka BP. The top of the core was set to the year of collection, AD 2015 (–65 cal yr BP).

Table 1. Radiocarbon ages from Pers and T3 lakes.

Core ID	Depth in sediment (cm)	Lab ID	Material dated	Fraction modern	δ^{13}C	Radiocarbon age (^{14}C yr BP)	Calibrated age (cal yr BP)
15-PLK-U3	16-17 cm	OS-125560	Plant	0.9594±0.0022	Not measured	335±20	390±75
15-PLK-U3	38-39 cm	OS-125561	Plant	0.9068±0.0019	Not measured	785±15	705±25
15-PLK-U3	90-91 cm	OS-125587	Plant	0.7677±0.0019	Not measured	2120±20	2080±70
*15-T1-U4	104-105 cm	OS-135047	Plant	0.3714±0.0065	—21.37	7690±35	8480±70
15-T3-U9	64-65 cm	OS-131813	Mollusk	0.2978±0.0008	Not measured	9730±20	10480±255

15-T3-U9	74-77 cm	OS-131812	Mollusk	0.2949±0.0011	Not measured	9810±30	10585±310
15-T3-U6	92-95 cm	OS-131814	Mollusk	0.3197±0.0009	Not measured	9160±20	9805±295

Marine reservoir correction applied (Delta-R= 115 ± 103). *Approximate isolation age of lake T1 (Lasher et al., 2020), see text for details. Calibrated ages are reported as midpoint of the 2σ range ± ½ of 2σ range.

4. Results and interpretations

4.1. Pers Lake

Core 15-PLK-U3 is subdivided into 4 units (1b, 1c, 2, 3, 4; Fig. 4). Core 15-PLK-U9 contains comparable units (1a, 1b, 1c, 2, 3, 4; Fig. 4) that are thinner because the core was sampled from a much shallower site with a slower sedimentation rate. The U9 core also contains an additional marine subunit, 1a. Unit 1a (core U9: 180-90 cm) is composed of massive gray silty-clays. The unit has very low organic matter content (averaging <1%). MS is medium-high, and Ti and Ca abundance is variable but relatively high. S concentration is very high at the bottom of the unit. Unit 1a is interpreted as a glacio-marine depositional environment. Unit 1b (core U3: 209-156 cm, core U9: 90-58 cm) is composed of gray silty-clay and very fine sand and becomes sandier toward the top of the unit. MS is low, Ti, Ca, and S concentrations are relatively high, and organic matter content is low (~1-2%). The combined evidence of very high S concentration (a primarily marine-sourced element) and low MS suggests that this unit represents a restricted marine phase with possible reduced mixing, stratification, and anoxia of dense, saline bottom waters (i.e. Balascio et al., 2011). Unit 1c (core U3: 156-145 cm, core U9: 58-50 cm) is composed of coarse sand to silt. MS is very high and organic matter content is low (dips to ~0.5%). Ti and Ca concentrations are relatively high. S concentration rapidly decreases through the unit indicating an abrupt decline in marine influence. Thus, unit 1c is interpreted as a transitional phase with possible intermittent marine influence by overtopping of the threshold and down-cutting through a now abandoned inflow delta. Between units 1c and 2, a light gray clay lamination at ~145 cm in core U3 (~50 cm in core U9) marks the marine-to-lacustrine transition.

Unit 2 (core U3: 145-110 cm, core U9: 50-37 cm) is composed of laminated brown, relatively organic rich lacustrine sediments (LOI increases to ~6-6.5%). MS is low and Ti and Ca concentrations are relatively reduced but increase toward the top of the unit in core U9. Unit 2 is interpreted as a period with no glacial melt water input (i.e. the GICs were either outside the Pers lake's catchment or completely melted away). Unit 3 (core U3: 110-66 cm, core U9: 37-20 cm) is composed of laminated sediments that are brown in color to grayer silty-clays at the top of the unit. There is a sandy layer at the beginning of the unit (~110 cm in core U3). MS is relatively low but variable. Organic matter content is variable but averages 4-5%. Ti concentration is variable—high at the beginning of the unit, then dips and generally increases toward the top of the unit. Unit 3 is interpreted as a period when the GICs were smaller than present or perhaps absent at times. Unit 4 (core U3: 66-0 cm, core U9: 20-0 cm) is composed of laminated silty to sandy clays that are brown to gray in color. MS is relatively high and organic matter content is relatively low (averaging ~3% in core U3 and less than ~1.5% in core U9). There are two short-lived increases in LOI at ~38 and ~16 cm in core U3 that are associated with mats of plant material. Ti and Ca concentrations are relatively high and increase at the top of the unit. Unit 4 is interpreted as a period with persistent glacial meltwater input.

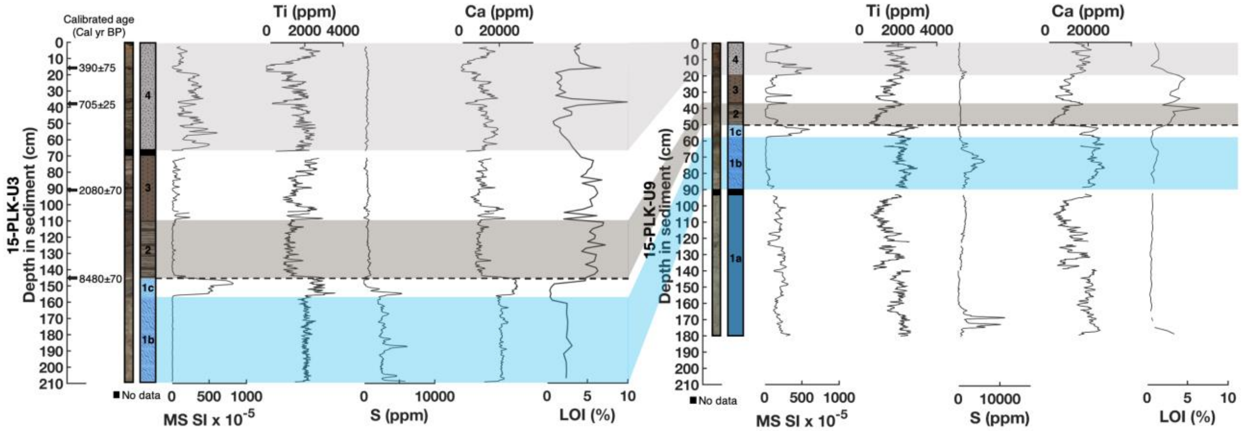

Figure 4. Pers lake core images, MS, Ti, S, and Ca concentration, and LOI. Unit 2 is interpreted as non-glacial conditions in the catchment. Presence vs. absence of local glaciers cannot be inferred below the marine-to-lacustrine transition (dashed line).

4.2. Lake T3

Core 15-T3-U9 is subdivided into three units (1a, 1b, 2, 3) and core 15-T3-U6 is subdivided into three comparable units (Fig. 5). At the base of the U9 core, a lower unit (151-100 cm) composed of reworked lacustrine material is excluded from the analysis. These sediments are located below marine sediments and we infer that they were suctioned into the core tube during core recovery. Unit 1a (core U9: 100-43 cm, core U6: 96-52cm) is composed of massive gray clays. Several mollusk shells were found within the unit along with several small rocks measuring ~1-3 cm in diameter. The unit has low organic matter content (less than 1%), high MS, and high Ti concentration. Ca and S concentrations are also relatively high and peak in the middle of the unit. This unit is indicative of a glacio-marine environment that was likely influenced by the rapidly retreating GrIS in the early Holocene. Unit 1b (core U9: 43-37 cm, core U6: 52-46 cm) is composed of laminated gray silty-clays. There is a coarse sand layer at the top of the unit between 38-37 cm in core U9 and between 47-46 cm in core U6. MS is relatively low, except for an increase at ~41 cm in core U9. Ti and Ca concentrations are relatively high but are reduced in the middle of the unit. S concentration is low but increases slightly at the top of the unit indicating some lingering marine influence. Organic matter content is higher than in unit 1a below but is still relatively low and does not exceed ~2%. Unit 1b is interpreted as a transitional phase with lessening marine influence.

To further constrain the marine-to-lacustrine transition in the Lake T3 cores, we measured percent carbon and nitrogen (%C, %N) and their isotope values ($\delta^{13}C$, $\delta^{15}N$) on bulk sediment samples (Fig. 6 and 7). Nitrogen isotope values ($\delta^{15}N$) are generally higher in the marine units in the T3 cores and range between 5 and 9 ‰. $\delta^{15}N$ values decrease from the marine to lacustrine units and range between 4 and 6.5 ‰ in the lacustrine units. Carbon isotope values ($\delta^{13}C$) values are generally higher in the marine units in the T3 cores and average –19.5‰ in core U9 and –19‰ in core U6 (one data point). $\delta^{13}C$ values generally decrease from the marine to lacustrine units to –23.5‰ at the top of core U9 and –23.9‰ at the top of core U6. In general, C:N values are lower in the marine sections of the T3 cores and higher in the lacustrine sections.

Unit 2 (core U9: 37-6 cm, core U6: 46-4 cm) is composed of laminated gray silty-clays and becomes more orange in color at the top of the unit. Organic matter content increases through the unit from <1 to ~4%. MS is low and Ti and Ca concentrations are ~1900 and ~20,000 ppm at the bottom of the unit, then generally decline through the unit. S concentration is minimal indicating a lacustrine environment post emergence of the basin. Unit 2 is interpreted as recording some GIC presence in the watershed, given overall low LOI (e.g., compared with the non-glacial unit 2 in the PLK cores). However, the data suggest a significant reduction in meltwater input and glacial extents throughout the duration of Unit 2 and relative to Unit 3 above. Unit 3 (core U9: 6-0, core U6: 4-0 cm) is composed of gray to orange-brown silty-clays. MS, Ti, and Ca concentrations are generally higher compared to the unit below. LOI decreases throughout Unit 3 in both core U9 and U6 to values ~3% at the core tops. Unit 3 is indicative of increased glacial extents and meltwater input.

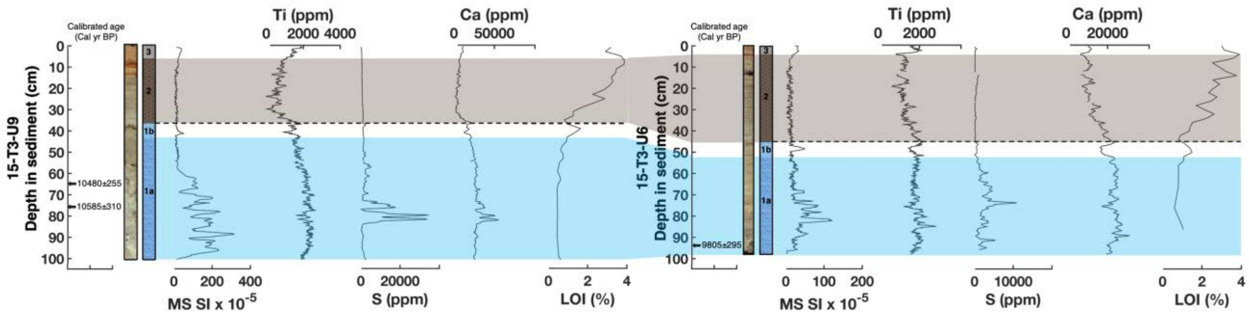

Figure 5. Lake T3 core images, MS, Ti, S, and Ca concentrations, and LOI. The dotted line shows the marine-to-lacustrine transition and isolation of the basin. Unit 2 is interpreted as a period with glacial meltwater input but significantly reduced GIC extents relative to Unit 3.

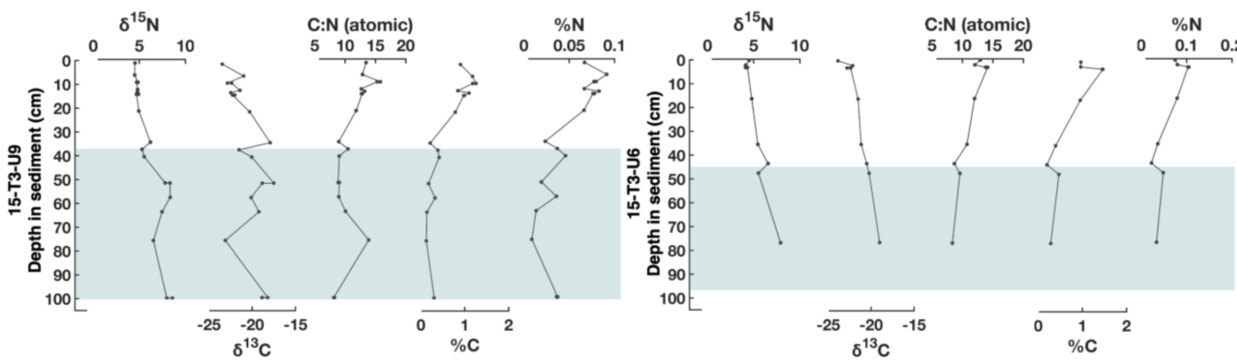

Figure 6. Bulk sediment composition from the Lake T3 cores plotted versus depth. From the left: δ^{15}N (‰ AIR), δ^{13}C (‰ VPDB), C:N (atomic ratio), %C and %N (bulk). The shaded blue region represents the marine and transitional units.

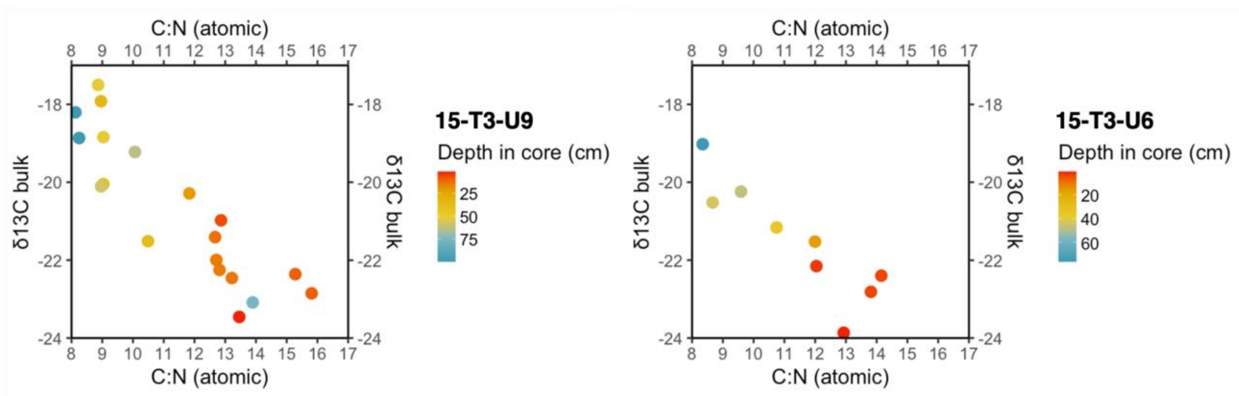

Figure 7. $\delta^{13}C$ (‰ VPDB) versus C:N in the Lake T3 cores with depth (color bar, red = core top, blue = core bottom).

5. Discussion

5.1. Regional deglaciation and emergence of lakes

Cosmogenic ^{10}Be exposure ages along a transect near Buksefjord suggest rapid retreat of the GrIS from the outer coast to the present-day ice margin in the early Holocene (between 10.7 ± 0.6 and 10.1 ± 0.4 ka BP) (Larsen et al., 2014). This suggests that the coastal, low elevation (~7 m a.s.l.) land from which Lake T3 subsequently formed was ice free by ~10.7 ka BP. Radiocarbon dates from marine shells in the Lake T3 cores support this result and show marine sedimentation at the site by at least ~10.6 ka BP. C:N values in the T3 basal units average <10 and $\delta^{13}C$ values range between –17 and –23 ‰ which is consistent with a predominantly marine organic matter source (Fig. 6) (Leng and Lewis, 2017). In addition, we suggest that the presence of small rocks in Lake T3's basal sediments along with some variability in %C, %N, and their isotope values (especially in the Lake T3 U9 core), may reflect the influence of ice-rafted debris and streamflow from the rapidly retreating GrIS. Although no marine shells were found in the Pers Lake cores, the physical and geochemical properties of the basal sediments (i.e. high S and Ca concentrations) also suggest a glacio-marine depositional environment and a relatively high sedimentation rate as a consequence of meltwater discharge from the rapidly retreating GrIS in the early Holocene.

Following deglaciation of the area, isostatic rebound caused local relative sea level to fall and the eventual isolation of Pers and T3 lakes from the sea. Both sites show evidence of a transitional period with lessening or intermittent marine influence before complete isolation of the basins. Due to a lack of dateable material, we approximate the timing of Pers Lake's isolation based on ^{14}C-dating of the hydrological isolation contact at nearby non-glacial Lake T1 (Fig. 2b). Lake T1 lies at a very similar elevation (~17.5 m a.s.l.) to Pers Lake (which lies at 20 m a.s.l.) and is located ~9 km southwest of Pers Lake and just north of Lake T3 (Lasher et al., 2020). Based upon the timing of Lake T1's emergence, our best estimate of Pers Lake's emergence is ~8.6 ka BP. A higher-elevation isolation lake (T2; 40 m a.s.l.) from the same study records emergence from the sea and lacustrine sedimentation earlier, likely ~9.4 ka BP (and definitely before 8.6-8.7 ka BP; Lasher et al., 2020). Other lake basins located near Nuuk were isolated from the sea at ~8.7 and ~8.5 ka BP and lie at 38 and 34 m a.s.l. respectively (Larsen et al., 2017).

The transition to a lacustrine environment at Lake T3 occurred after ~9.8 ka BP (the youngest ^{14}C age from the marine sediments). As direct age control on the Lake T3 cores is very limited due to the dearth of ^{14}C-dateable organic materials in the lacustrine units, we infer the isolation age of Lake T3 using a wider range of regional relative sea level (RSL) data from nearby isolation basins as well as dated marine shell fragments from surface glacio-marine deposits (Weidick, 1976; Fredskild, 1983; Larsen et al., 2017; Lasher et al., 2020; Fig. 8). In general, RSL data from Outer Nuuk Fjord, Kobbefjord and Buksefjord (which includes locations up to 80 km away), although slightly different in the timing, all suggest rapid early Holocene RSL fall in this region (Fig. 8). None of the lake data was collected specifically with RSL reconstructions in mind which explains the large altitude uncertainties on the individual index points, and as they are from different locations the spread of data is also likely due to differential glacio-isostatic adjustment across the region during the early Holocene. Although we know that RSL was rapidly falling during the early Holocene, the timing of RSL reaching close to present in this region is less well constrained. Despite this, marine shell data from Outer Nuuk Fjord, the rapid RSL fall seen between lakes T2 and T1 in Buksefjord, and the timing of isolation of Lake T1 all suggest that RSL was likely close to present in Buksefjord by c. 8 ka BP (Fig. 8). This rapid RSL fall appears to be earlier and potentially more rapid than at Kobbefjord or Outer Nuuk Fjord but the caveats about these other data points mean we should focus on the Buksefjord data to constrain when lake T3 was isolated, rather than the regional RSL dataset.

Focusing on estimating the timing of isolation of Lake T3 (at 7 m a.s.l.), we know that it cannot have occurred before ~8.5 ka BP because this is the timing of isolation in Lake T1, situated only 600 m away and 10.5 m higher in the landscape. This index point fits closely with other regional RSL data (Fig. 8). We therefore suggest that Lake T3 was isolated sometime between 8.4 and 7.5 ka BP. This assumes a linear rate of RSL fall between lakes T2, T1 and T3 (grey arrow in Fig. 8) which gives an isolation age between c. 8.4 – 8 ka BP (using the dating uncertainty on lake T2 isolation as a guide), but we also extend the lower age limit of T3 isolation by 500 years to allow for the possibility that RSL slowed down as it came closer to present, which is a common feature of west Greenland Holocene RSL curves (e.g. Sisimiut area - Bennike et al., 2011, Long et al., 2011), but becomes less pronounced moving south along the west coast (e.g. Paamiut area - Woodroffe et al., 2014) (dashed grey box in Fig. 8). Although using this method means that the Lake T3 core chronologies are less robust than for Pers Lake, they do demonstrate that the lacustrine sediment records likely span from the early/middle Holocene to the present.

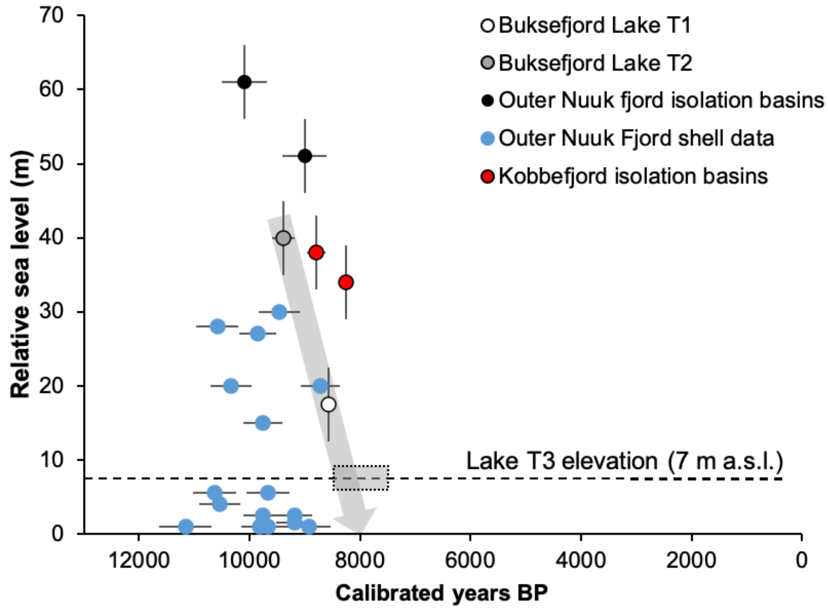

Figure 8. RSL reconstructions from Outer Nuuk fjord (black dots) and Kobbefjord (red dots) isolation basins and marine limiting data from dated shell fragments (blue dots) in the Nuuk region. T1 (white dot) and T2 (gray dot) data are from Lasher et al., 2020; Outer Nuuk Fjord data are from Fredskild, 1983, Larsen et al., 2017; and the marine shell fragment data are from Weidick, 1976. The dashed line shows the elevation of Lake T3, the gray arrow shows the estimated regional early Holocene RSL curve and the dashed grey box shows the estimated timing of isolation of Lake T3 between ~8.4 and 7.5 ka BP.

5.2. GIC fluctuations and Holocene climate of southwest Greenland

Here we summarize Holocene climate trends in southwest Greenland inferred from GIC reconstructions at Lake T3 and Pers Lake. We also compare our results with other regional GIC records and temperature sensitive paleoclimate records. Following the marine-to-lacustrine transition in Pers Lake at ~8.6 ka BP, the deposition of brown, laminated, and relatively organic-rich sediment suggests no local glacial meltwater input at this time, and that upstream GICs were either retreated beyond that lake's catchment, or more likely, completely melted away. We note that ~8.6 ka BP is a minimum limiting age on local GIC disappearance from the Pers Lake catchment, as we cannot assess whether glacier meltwater input ceased sometime before isolation from the sea. However, a nearby study shows some lingering glacial influence in the early-to-middle Holocene in this region. Glacial lake IS21, ~45 km to the north (Fig. 9E) formed before ~9 ka BP (and ~1.7 ka after deglaciation of the local area) and received meltwater inflow from a local glacier until ~7.9 ka BP (Larsen et al., 2017).

Conversely, following emergence of Lake T3 between ~8.4-7.5 ka BP, the sediment record there suggests continuous glacial meltwater input through the remainder of the Holocene. Geochemical data from Lake T3 do suggest an extended period (of unknown age and duration) of significantly reduced meltwater input and GIC extents after isolation of the basin. Still, the inorganic nature of the sediments suggests that at least some glacial ice was probably present throughout the lacustrine period. Like at Pers Lake, we cannot infer the status of local GICs from the marine sediments at T3, because this marine site also could have received glacial sediments from tidewater outlets of the GrIS. We cannot rule out that local GICs were absent or completely melted away prior to Lake T3's isolation from the sea. However, we think this is unlikely because the majority of regional temperature sensitive proxy records register cooling in the middle Holocene, ~5 ka BP, and no earlier than ~7 ka BP (Fig. 9). Thus, if Lake T3's GICs were absent before the lake's isolation, this would require GIC regrowth much earlier than when most records suggest cooling temperatures.

Together, the initial timing of glacial meltwater reduction at Lake T3 and disappearance of GICs from the Pers Lake catchment from at least ~8.6 and until ~4.3 ka BP indicate warmer-than-present summer temperatures in southwest Greenland in the early-to-middle Holocene. This agrees with the majority of other regional paleoclimate records that show warmer-than-present conditions between ~9-5 ka BP (Fig. 9). More positive $\delta^{18}O$ values from adjacent non-glacial lakes T1 and T2 indicate warmer-than-present temperatures by at least ~9 ka BP, and the onset of peak warmth between ~9.4 and 8.8 ka BP (Fig. 9G; Lasher et al., 2020). Rising temperatures are inferred from pollen assemblages in the Godthåbsfjord area from ~9 ka BP onwards, and suggest that growing season temperatures had reached today's values between ~8 and 7.5 ka BP (Fig. 9L; Fredskild, 1983), though we note the possibility of a lag relative to climate due to plant species migration timing. Farther away, ~340 km to the northwest between coastal Sisimuit and inland Kangerlussuaq fjord, sediment records of β carotene, a proxy for aquatic production, from four lakes suggest maximum biological production and maximum warmth between ~8.5-5 ka BP (Fig. 9H; Law et al., 2015). Reconstructed chlorophyll-*a* shows maximum biological production at ~8 ka BP, and generally high production between ~9-5.3 ka BP, and diatom assemblages from the same study suggest an early and dry period until ~5.6 ka BP (Fig. 9I; Perren et al., 2012). Other sediment records from the Sisimuit area also suggest an early-middle HTM from ~10 to 4.5 ka BP, reflected by warmth-demanding aquatic plants and invertebrates (Fig. 9J; Wagner and Bennike, 2012). A lake sediment record spanning the last ~8.2 ka years infers peak summer temperatures at ~7-6.5 ka BP from the presence of shells of the boreal ostracod *Ilyocypris bradyi* (Fig. 9K; Bennike et al., 2010). Along with warmth, several studies suggest more evaporative conditions in southwest Greenland during the HTM. A stable isotope ($\delta^{18}O$ and $\delta^{13}C$) record from two lakes near Kangerlussuaq show arid conditions between ~7-5.6 ka BP (Anderson and Leng, 2004; McGowan et al., 2003), and a reconstructed lake level curve for Hunde Sø (also near Kangerlussuaq) suggests low lake levels due to dry conditions between ~7.4-6 ka BP (Aebly and Fritz, 2009). However, it is possible that this effect is localized given the large climatic gradient between coastal and inland areas.

Other local glacier reconstructions from the region largely agree with the timing of GIC disappearance or reduction seen in the Pers Lake and Lake T3 records. Closest to our sites, three proglacial threshold lake records near Nuuk show that glacial meltwater ceased and that glaciers melted away completely due to high local summer air temperatures between ~8.7 and 7.9 ka BP (Fig. 1B and 9C, D, & E; Larsen et al., 2017). Approximately 210 km north of Buksefjord, a proglacial lake record of fluctuations of GICs adjacent to Sukkertoppen Iskappe suggests GIC retreat between ~9.3-4.6 ka BP. Geochemical data also suggest that there may have been a small amount of lingering ice in the lake catchment until ~8 ka BP (Fig. 1B and 9F; Schweinsberg et al., 2018). Combined with our two records, the existing GIC records from southwest Greenland (i.e. Larsen et al., 2017; Schweinsberg et al., 2018) suggest initial GIC retreat or absence in the early-to-middle Holocene, between ~9.3-7.5 ka BP. Moreover, the onset of organic-rich sedimentation and inferred complete disappearance of the GICs within the Pers, Badesø, Langesø, and IS21 lake catchments between at least ~8.7 and ~7.9 ka BP indicates warmer-than-present conditions during this period.

Following the warmer-than-present HTM, existing records suggest cooling and GIC expansion in the late Holocene (Briner et al., 2016; Larsen et al., 2019). We record renewed ice growth at Pers Lake by ~4.3 ka BP, but variable LOI and geochemical data suggest that GICs were either smaller than present or completely absent at times (Fig. 9A) until ~1.4 ka BP. Persistent GICs were present inside the Pers Lake catchment beginning ~1.4 ka BP, the timing of which is in agreement with several other GIC records from the North Atlantic region (i.e. van der Bilt et al., 2019). Nearby, at Crash lake, an interval of glacier expansion is recorded at ~1.2 ka BP

(Schweinberg et al., 2018) and at lake IS21 an advance is recorded between ~1.6-1.4 ka BP (Larsen et al., 2017). Geochemical data at Pers Lake reflect maximum minerogenic input ~0.1 ka BP. Thus, we infer maximum ice extents at Pers Lake late in the LIA. Similarly, data from the Lake T3 cores also suggest an increase in GIC extents toward the top of the record. However, due to dating limitations we cannot determine the timing of this GIC growth (Fig. 9B).

Other temperature sensitive paleoclimate proxies also indicate middle-to-late Holocene cooling, albeit with variable timing. The nearby T1 and T2 lake records show a gradual trend toward more negative lake water (precipitation) $\delta^{18}O$ values after ~7 ka BP and suggest 2 to 4°C of gradual cooling from the early to late Holocene (Fig. 10), although the study does not strictly quantify temperature changes or summer temperatures (Lasher et al., 2020). $\delta^{18}O$ values in the T1 and T2 lake records also show a marked decline from ~2.5 ka BP and minimum values between ~1.4-1.2 ka BP (Fig. 10), which is in very good agreement with the inferred reappearance of persistent ice in the Pers lake catchment at ~1.4 ka BP. Pollen assemblages suggest that cold conditions set in by ~3.6 ka BP in the Nuuk area, followed by a further deterioration between ~2.5 and 2 ka BP (Fig. 9L; Fredskild, 1983). Law et al. (2015) report a progressive decline in β carotene from ~5 ka BP at four lakes, which is interpreted as the onset of colder and wetter conditions (Fig. 9H). Reconstructed chlorophyll-*a* suggests a transition to a more moist, cooler, and a windier climate between ~5.6-4 ka BP, and diatom assemblages suggest that Neoglacial conditions began ~4.5 ka BP (Fig. 9I; Perren et al., 2012). A set of Sisimiut sediment records show cooler and less arid summers from ~5 ka BP (Fig 8J; Wagner and Bennike, 2012). Correspondingly, Leng et al. (2012) report increased input of terrestrial organic matter into a small freshwater lake near Sisimiut and infer Neoglacial cooling between ~5.5-1 ka BP. In addition to cooling, several studies suggest a shift to wetter conditions in the middle-to-late Holocene. McGowan et al. (2003) find a period of positive effective precipitation between ~5.6-4.7 ka BP, and reconstructed lake levels suggest two pluvial periods at ~4.6 and ~2 ka BP (Aebly and Fritz, 2009).

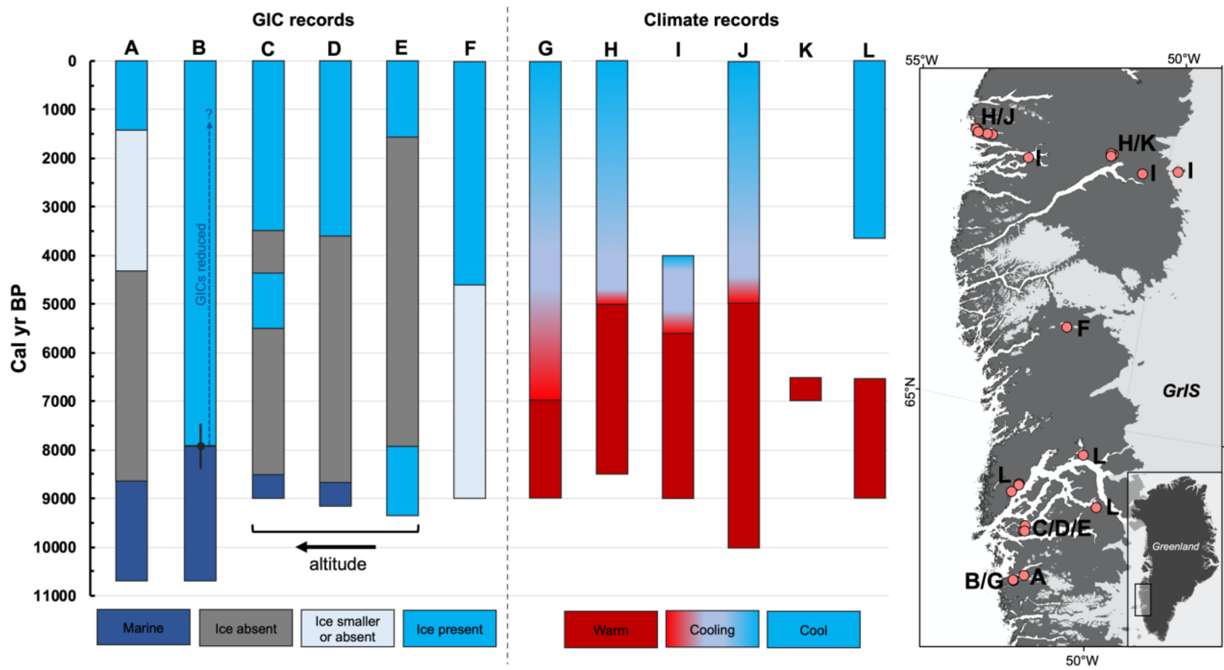

Figure 9. Summary of southwest Greenland GIC records and other temperature sensitive paleoclimate reconstructions. A. Pers Lake and B. Lake T3 (this study); C. Badesø Lake, D. Langesø Lake, and E. Lake IS21 (Larsen et al., 2017); F. Crash Lake (Schweinsberg et al., 2018); G. $\delta^{18}O$ (Lasher et al., 2020); H. β carotene (Law et al., 2015); I. Chlorophyll-*a* and diatom assemblages (Perren et al., 2012); J. Warm indicator bryozoans (Wagner and Bennike, 2012); K. Shells of the ostracod *Ilyocypris bradyi* (Bennike et al., 2010); L. Pollen assemblages (Fredskild, 1983). Note the timing of reduced GICs at Lake T3 is approximate.

5.3. Regional Holocene GIC ELAs

Thus far, other than the high elevation Renland ice cap in the frigid mid-Arctic climate of central east Greenland, the Lake T3 record is the first to infer possible local GIC survival through the Holocene in the southern half of Greenland (Larsen et al., 2019; Larocca at al., 2020). We suggest that ice within the Lake T3 catchment was able to survive the HTM due to its high elevation. This unique record allows for a maximum bound on regional GIC ELAs to be estimated. Based on our lake records and present-day ice elevations, we can first infer that regional GIC ELAs were likely higher than ~975 m a.s.l. and lower than ~1470 m a.s.l. in the early-to-middle Holocene. We base the maximum constraint on ELA (i.e. ~1470 m a.s.l.) on the T3 Lake record, which shows that some ice probably remained in the lake's catchment through the Holocene. Thus, GIC ELAs must not have risen above the highest present-day ice elevation at this site. ELAs greater than ~1470 m a.s.l. would have led to organic sedimentation at Lake T3, which is not seen in the sediment record. Our minimum constraint on ELA (i.e. ~975 m a.s.l.) is based on the Pers lake record, which suggests that all glacier ice had melted beyond the lake catchment by at least ~8.6 ka BP. Thus, GIC ELAs must have been greater than ~975 m a.s.l. in the early-to-middle Holocene. The three proglacial threshold lake records from the Kobbefjord area support our ELA constraints and show that the GICs (with present-day maximum ice elevations between 1000-1370 m a.s.l.) melted away completely in the early-to-middle Holocene (Larsen et al., 2017). Inclusion of these additional records suggest that regional GIC ELAs were greater than ~1370 m a.s.l. and less than ~1470 m a.s.l. during peak warmth (Fig. 10).

Larsen et al. (2017) found that GIC regrowth first initiated on the highest elevation peaks at Kobbefjord, which suggests progressive ELA lowering during the Neoglacial. According to their study, regional GIC ELAs were likely less than ~1370 m a.s.l by ~5.5 ka BP, less than ~1170 m a.s.l. by ~3.6 ka BP, and less than ~1000 m a.s.l. by ~1.6 ka BP (Fig. 9C, D, & E and Fig. 10). Geochemical evidence from Crash lake suggests the onset of Neoglaciation at ~4.6 ka BP, and further snowline lowering on ice caps around Sukkertopeen Iskappe at ~3.7, ~3.0, ~1.8, ~1.2, and ~0.7 ka BP, however ice elevation ranges were not reported (Fig. 9F; Schweinsberg et al., 2018).

Our results support this successive glacier expansion and suggest a further ELA lowering to less than ~975 m a.s.l. by ~1.4 ka BP, when persistent GICs are first inferred within the Pers Lake catchment (Fig. 10). Over the middle-to-late Holocene, these combined results suggest an overall, gradual ELA lowering of ~400 m. Making the assumption that precipitation remained constant through the Holocene, the summer temperature change responsible for this ELA shift can be roughly estimated at ~2.7ºC of cooling between ~5.5 and ~1.4 ka BP (using an average atmospheric lapse rate of 0.68ºC/100 meters) (e.g., Nesje et al., 1991; Dahl and Nesje, 1992; Fausto et al., 2009). However, we acknowledge the that the amount of precipitation and/or precipitation seasonality may have changed through the Holocene (i.e. Thomas et al., 2016; 2018). For reference, we also assessed modern GIC ELAs in the Pers and T3 lake catchments (Fig. 10) by averaging late summer (July, August, and/or September) snowlines between the years 1987-2019. Snowline elevations were constrained by digitizing the line in which white snow meets glacial ice from cloud-free Landsat imagery using the Google Earth Engine Digitisation Tool (GEEDiT) (Lea, 2018) and the ASTER DEM was used to extract the mean snowline elevation.

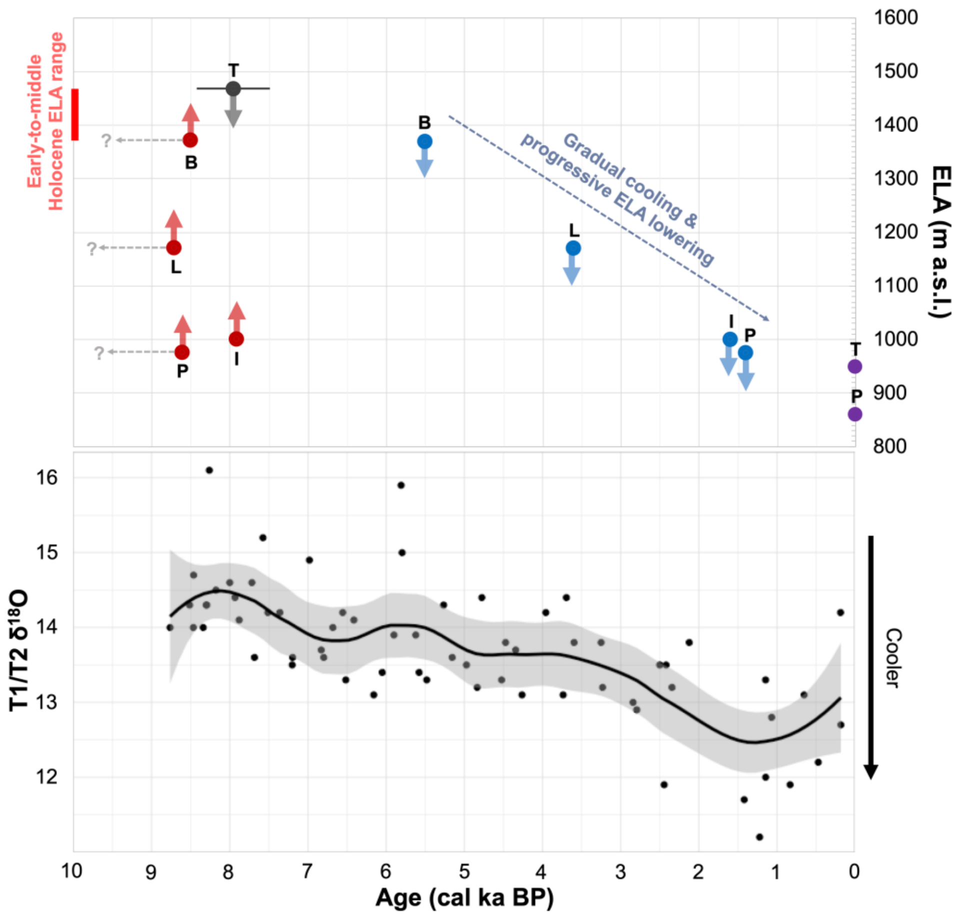

Figure 10. Top: Southwest Greenland ELA constraints from lakes Badesø (B), Langesø (L), and Lake IS21 (I) (Larsen et al., 2017) and Pers Lake (P) and Lake T3 (T) (this study). Blue points indicate timing of glacier regrowth in lake catchments and a maximum constraint on ELA (i.e. ELAs must have been lower for glaciers to have appeared in the lake catchments). Red points indicate timing of glacier disappearance from lake catchments and a minimum constraint on ELA (i.e. ELAs must have been higher for ice to have exited catchments). Gray point indicates maximum elevation of extant ice in the T3 watershed, a maximum constraint on early-to-middle Holocene ELA (because glacier meltwater influx to T3 probably persisted through the Holocene). We use the median of our isolation age estimate for lake T3, i.e. ~7.95 ka BP (the full age estimate, ~8.4-7.5 ka BP, is denoted by the gray horizontal bar). Purple points show the estimated modern

ELA for the GICs within the Pers and T3 lake catchments as comparison to Holocene ELA inferences (860 and 950 m a.s.l. respectively). The vertical light red bar is the estimated ELA range during peak warmth, >1370 and <1470 m a.s.l. The timing of glacier disappearance from Badesø, Langesø (Larsen et al., 2017), and Pers Lake (this study) is based upon the date of isolation from the sea, thus we cannot assess whether glacial meltwater influx ceased during the isolation or sometime before then (horizontal gray arrows). Bottom: Combined chironomid $\delta^{18}O$ (‰ VSMOW) from lake T1 and T2 (Lasher et al., 2020).

6. Conclusions

In this study, we present two continuous, Holocene-length lake sediment records of GIC fluctuations from southwest Greenland. GICs within the Pers and T3 lake catchments varied in size significantly through the Holocene. We find that GICs in the Pers Lake catchment were likely completely melted away from at least ~8.6 ka BP (the lake's isolation from the sea) to ~4.3 ka BP, and that the GICs fluctuated between smaller than present or absent between ~4.3 and ~1.4 ka BP. At nearby Lake T3, which has larger and higher elevation GICs in its catchment, at least some ice probably persisted throughout the HTM (with the caveat that we cannot evaluate presence or absence of local glaciers near Lake T3 before ~8.4-7.5 ka BP). This result is in contrast to other GIC records from the southern half of Greenland that show most GICs melted away completely during the HTM. These two watersheds thus provide upper and lower bounds on ELAs during the early-to-middle Holocene warm period, namely that regional GIC ELAs were higher than ~975 m a.s.l. and lower than ~1470 m a.s.l. Combined with other regional GIC records, which show GICs disappearing at even higher elevations than that of the Pers Lake glacier, we estimate regional GIC ELAs were between ~1370 and ~1470 m a.s.l. during peak HTM warmth. Geochemical and physical sedimentary evidence suggest increased glacial meltwater input at the top of the Lake T3 record, and regrowth and persistent meltwater input at Pers Lake by ~1.4 ka BP. This result is in agreement with gradual Neoglacial cooling and progressive ELA lowering to <975 m a.s.l. in the late Holocene, driven by a decline in Northern Hemisphere summer insolation. We estimate an overall middle-to-late Holocene ELA lowering of ~400 m, which corresponds to ~2.7ºC of summer cooling assuming no change in precipitation. At ~0.1 ka BP, we find increased minerogenic input at Pers Lake, indicating maximum GIC extent during the latest part of the LIA, although in the present study we cannot estimate ELAs for that time. Given the sensitive response of GICs to climate variations through the Holocene, we expect that the region's GICs will continue to retreat as a consequence of ongoing anthropogenic warming. Ultimately, improved knowledge of the Holocene history of Greenland's GICs will help to place the recent retreat of Greenland's outlying glaciers into a longer-term perspective, and to improve the forecasting of future ice loss in the region.

Acknowledgments

This research was supported by National Geographic Society grant 9694-15 and U.S. National Science Foundation (NSF) Polar Programs CAREER grant 1454734 awarded to YA, NSF Geography and Spatial Sciences DDRI grant 1812764 awarded to LL and YA, and Northwestern University undergraduate research assistant program (URAP) funds that supported BG. We thank S. Funder for sharing relative sea-level data; A. Masterson, G. Schellinger, K. Berman, and P. Kotecki for lab access and assistance; Woods Hole Oceanographic Institution–National Ocean Sciences Accelerator Mass Spectrometry facility for radiocarbon analysis; the United States Geological Survey (USGS) and the Polar Geospatial Center (PGC) for satellite imagery; S.

Ólafsdóttir and B. Gray for field assistance and T. Axford for building field equipment. We thank the people and the Government of Greenland for site access (under scientific survey license VU-00090 and export permit 062/2015) and Pinngortitaleriffik (Greenland Institute of Natural Resources) and M. Rosen for essential field support. Geospatial support for this work provided by PGC under NSF-OPP awards 1043681 and 1559691. We thank Nicolaj Krog Larsen and one anonymous reviewer for improving this manuscript.

References

Aebly, F.A., Fritz, S.C., 2009. Palaeohydrology of Kangerlussuaq (Søndre Strømfjord), West Greenland during the last ~8000 years. The Holocene 19, 91–104. doi:10.1177/0959683608096601

Anderson, N., Leng, M.J., 2004. Increased aridity during the early Holocene in West Greenland inferred from stable isotopes in laminated-lake sediments. Quaternary Science Reviews 23, 841–849. doi:10.1016/j.quascirev.2003.06.013

Axford, Y., Lasher, G., Kelly, M., Osterberg, E., Landis, J., Schellinger, G., Pfeiffer, A., Thompson, E., Francis, D., 2019. Holocene temperature history of northwest Greenland – With new ice cap constraints and chironomid assemblages from Deltasø. Quaternary Science Reviews 215, 160–172. doi:10.1016/j.quascirev.2019.05.011

Balascio, N.L., Dandrea, W.J., Bradley, R.S., 2015. Glacier response to North Atlantic climate variability during the Holocene. Climate of the Past Discussions 11, 2009–2036. doi:10.5194/cpd-11-2009-2015

Balascio, N.L., Zhang, Z., Bradley, R.S., Perren, B., Dahl, S.O., Bakke, J., 2011. A multi-proxy approach to assessing isolation basin stratigraphy from the Lofoten Islands, Norway. Quaternary Research 75, 288–300. doi:10.1016/j.yqres.2010.08.012

Bennike, O., Anderson, N.J., Mcgowan, S., 2010. Holocene palaeoecology of southwest Greenland inferred from macrofossils in sediments of an oligosaline lake. Journal of Paleolimnology 43, 787–798. doi:10.1007/s10933-009-9368-x

Bennike, O., Wagner, B., Richter, A., 2011. Relative sea level changes during the Holocene in the Sisimiut area, south-western Greenland. Journal of Quaternary Science 26, 353–361. doi:10.1002/jqs.1458

Bjørk, A.A., Kjær, K.H., Korsgaard, N.J., Khan, S.A., Kjeldsen, K.K., Andresen, C.S., Box, J.E., Larsen, N.K., Funder, S., 2012. An aerial view of 80 years of climate-related glacier fluctuations in southeast Greenland. Nature Geoscience 5, 427–432. doi:10.1038/ngeo1481

Blaauw, M., Christen, J.A., 2011. Flexible paleoclimate age-depth models using an autoregressive gamma process. Bayesian Analysis 6, 457–474. doi:10.1214/11-ba618

Briner, J.P., Mckay, N.P., Axford, Y., Bennike, O., Bradley, R.S., Vernal, A.D., Fisher, D., Francus, P., Fréchette, B., Gajewski, K., Jennings, A., Kaufman, D.S., Miller, G., Rouston, C., Wagner, B., 2016. Holocene climate change in Arctic Canada and Greenland. Quaternary Science Reviews 147, 340–364. doi:10.1016/j.quascirev.2016.02.010

Cappelen, J., 2018. Greenland-Dmi Historical Climate Data Collection 1784-2017. *DNI Report 18-04*.

Dahl, S.O., Bakke, J., Lie, Ø., Nesje, A., 2003. Reconstruction of former glacier equilibrium-line altitudes based on proglacial sites: an evaluation of approaches and selection of sites. Quaternary Science Reviews 22, 275–287. doi:10.1016/s0277-3791(02)00135-x

Dahl, S.O., Nesje, A., 1992. Paleoclimatic implications based on equilibrium-line altitude depressions of reconstructed Younger Dryas and Holocene cirque glaciers in inner Nordfjord, western Norway. Palaeogeography, Palaeoclimatology, Palaeoecology 94, 87–97. doi:10.1016/0031-0182(92)90114-k

D'Andrea, W.J., Huang, Y., Fritz, S.C., Anderson, N.J., 2011. Abrupt Holocene climate change as an important factor for human migration in West Greenland. Proceedings of the National Academy of Sciences 108, 9765–9769. doi:10.1073/pnas.1101708108

Dietrich, G., 1980. General oceanography: an introduction. Wiley, New York.

Fausto, R.S., Ahlstrøm, A.P., As, D.V., Bøggild, C.E., Johnsen, S.J., 2009. A new present-day temperature parameterization for Greenland. Journal of Glaciology 55, 95–105. doi:10.3189/002214309788608985

Fredskild, B., 1983. The Holocene vegetational development of the Godthåbsfjord area, West Greenland. Commission for Scientific Research in Greenland.

GEUS, 2018. Geological map of South, South-West and southern West Greenland 1:100,000. Geological Survey of Denmark and Greenland (GEUS), maps.greenmin.gl/geusmap/.

Heiri, O., Lotter, A.F. and Lemcke, G., 2001. Loss on ignition as a method for estimating organic and carbonate content in sediments: reproducibility and comparability of results. Journal of paleolimnology, 25(1), pp.101-110. doi:10.1023/A:1008119611481

Kaufman, D., 2004. Holocene thermal maximum in the western Arctic (0–180°W). Quaternary Science Reviews 23, 529–560. doi:10.1016/j.quascirev.2003.09.007

Kelly, M.A., Lowell, T.V., 2009. Fluctuations of local glaciers in Greenland during latest Pleistocene and Holocene time. Quaternary Science Reviews. 28, 2088-2106. doi:10.1016/j.quascirev.2008.12.008.

Larocca, L.J., Axford, Y., Bjørk, A.A., Lasher, G.E., Brooks, J.P., 2020. Local glaciers record delayed peak Holocene warmth in south Greenland. Quaternary Science Reviews 241, 106421. doi:10.1016/j.quascirev.2020.106421

Larsen, N.K., Funder, S., Kjær, K.H., Kjeldsen, K.K., Knudsen, M.F., Linge, H., 2014. Rapid early Holocene ice retreat in West Greenland. Quaternary Science Reviews 92, 310–323. doi:10.1016/j.quascirev.2013.05.027

Larsen, N.K., Strunk, A., Levy, L.B., Olsen, J., Bjørk, A., Lauridsen, T.L., Jeppesen, E., Davidson, T.A., 2017. Strong altitudinal control on the response of local glaciers to Holocene climate change in southwest Greenland. Quaternary Science Reviews 168, 69–78. doi:10.1016/j.quascirev.2017.05.008

Larsen, N.K., Levy, L.B., Strunk, A., Søndergaard, A.S., Olsen, J., Lauridsen, T.L., 2019. Local ice caps in Finderup Land, North Greenland, survived the Holocene Thermal Maximum. Boreas 48, 551–562. doi:10.1111/bor.12384

Lasher, G.E., Axford, Y., Masterson, A.L., Berman, K., Larocca, L.J., 2020. Holocene temperature and landscape history of southwest Greenland inferred from isotope and geochemical lake sediment proxies. Quaternary Science Reviews 239, 106358. doi:10.1016/j.quascirev.2020.106358

Law, A., Anderson, N., Mcgowan, S., 2015. Spatial and temporal variability of lake ontogeny in south-western Greenland. Quaternary Science Reviews 126, 1–16. doi:10.1016/j.quascirev.2015.08.005

Lea, J.M., 2018. The Google Earth Engine Digitisation Tool (GEEDiT) and the Margin change Quantification Tool (MaQiT) – simple tools for the rapid mapping and quantification of changing Earth surface margins. Earth Surface Dynamics 6, 551–561. doi:10.5194/esurf-6-551-2018

Lecavalier, B.S., Milne, G.A., Simpson, M.J., Wake, L., Huybrechts, P., Tarasov, L., Kjeldsen, K.K., Funder, S., Long, A.J., Woodroffe, S., Dyke, A.S., Larsen, N.K., 2014. A model of Greenland ice sheet deglaciation constrained by observations of relative sea level and ice extent. Quaternary Science Reviews 102, 54–84. doi:10.1016/j.quascirev.2014.07.018

Leclercq, P.W., Weidick, A., Paul, F., Bolch, T., Citterio, M., Oerlemans, J., 2012. Brief communication: Historical glacier length changes in West Greenland. The Cryosphere Discussions 6, 3491–3501. doi:10.5194/tcd-6-3491-2012

Leng, M.J., Lewis, J.P., 2017. C/N ratios and Carbon Isotope Composition of Organic Matter in Estuarine Environments. Applications of Paleoenvironmental Techniques in Estuarine Studies Developments in Paleoenvironmental Research 213–237. doi:10.1007/978-94-024-0990-1_9

Leng, M.J., Wagner, B., Anderson, N.J., Bennike, O., Woodley, E., Kemp, S.J., 2012. Deglaciation and catchment ontogeny in coastal south-west Greenland: implications for terrestrial and aquatic carbon cycling. Journal of Quaternary Science 27, 575–584. doi:10.1002/jqs.2544

Levy, L.B., Kelly, M.A., Lowell, T.V., Hall, B.L., Hempel, L.A., Honsaker, W.M., Lusas, A.R., Howley, J.A., Axford, Y.L., 2014. Holocene fluctuations of Bregne ice cap, Scoresby Sund, east Greenland: a proxy for climate along the Greenland Ice Sheet margin. Quaternary Science Reviews 92, 357–368. doi:10.1016/j.quascirev.2013.06.024

Long, A.J., Woodroffe, S.A., Roberts, D.H., Dawson, S., 2011. Isolation basins, sea-level changes and the Holocene history of the Greenland Ice Sheet. Quaternary Science Reviews 30, 3748–3768. doi:10.1016/j.quascirev.2011.10.013

Lowell, T.V., Hall, B.L., Kelly, M.A., Bennike, O., Lusas, A.R., Honsaker, W., Smith, C.A., Levy, L.B., Travis, S., Denton, G.H., 2013. Late Holocene expansion of Istorvet ice cap, Liverpool Land, east Greenland. Quaternary Science Reviews 63, 128–140. doi:10.1016/j.quascirev.2012.11.012

Machguth, H., Rastner, P., Bolch, T., Mölg, N., Sørensen, L.S., Aðalgeirsdottir, G., Angelen, J.H.V., Broeke, M.R.V.D., Fettweis, X., 2013. The future sea-level rise contribution of Greenland’s glaciers and ice caps. Environmental Research Letters 8, 025005. doi:10.1088/1748-9326/8/2/025005

McGowan, S., Ryves, D.B., Anderson, N.J., 2003. Holocene records of effective precipitation in West Greenland. The Holocene 13, 239–249. doi:10.1191/0959683603hl610rp

Möller, P., Larsen, N.K., Kjær, K.H., Funder, S., Schomacker, A., Linge, H., Fabel, D., 2010. Early to middle Holocene valley glaciations on northernmost Greenland. Quaternary Science Reviews 29, 3379–3398. doi:10.1016/j.quascirev.2010.06.044

Nesje, A., Dahl, S.O., Andersson, C., Matthews, J.A., 2000. The lacustrine sedimentary sequence in Sygneskardvatnet, western Norway: a continuous, high-resolution record of the Jostedalsbreen ice cap during the Holocene. Quaternary Science Reviews 19, 1047–1065. doi:10.1016/s0277-3791(99)00090-6

Nesje, A., Kvamme, M., Rye, N. and Løvlie, R., 1991. Holocene glacial and climate history of the Jostedalsbreen region, western Norway; evidence from lake sediments and terrestrial deposits. Quaternary Science Reviews 10, 87-114. doi:10.1016/0277-3791(91)90032-P

Oerlemans, J., 2001. Glaciers and climate change. Balkema, Lisse.

Oerlemans, J., 2005. Extracting a Climate Signal from 169 Glacier Records. Science 308, 675–677. doi:10.1126/science.1107046

Perren, B.B., Anderson, N.J., Douglas, M.S.V., Fritz, S.C., 2012. The influence of temperature, moisture, and eolian activity on Holocene lake development in West Greenland. Journal of Paleolimnology 48, 223–239. doi:10.1007/s10933-012-9613-6

Rastner, P., Bolch, T., Mölg, N., Machguth, H., Bris, R.L., Paul, F., 2012. The first complete inventory of the local glaciers and ice caps on Greenland. The Cryosphere 6, 1483–1495. doi:10.5194/tc-6-1483-2012

Raup, B., Racoviteanu, A., Khalsa, S.J.S., Helm, C., Armstrong, R., Arnaud, Y., 2007. The GLIMS geospatial glacier database: A new tool for studying glacier change. Global and Planetary Change 56, 101–110. doi:10.1016/j.gloplacha.2006.07.018

Reimer, P.J., Bard, E., Bayliss, A., Beck, J.W., Blackwell, P.G., Ramsey, C.B., Buck, C.E., Cheng, H., Edwards, R.L., Friedrich, M., Grootes, P.M., Guilderson, T.P., Haflidason, H., Hajdas, I., Hatté, C., Heaton, T.J., Hoffmann, D.L., Hogg, A.G., Hughen, K.A., Kaiser, K.F., Kromer, B., Manning, S.W., Niu, M., Reimer, R.W., Richards, D.A., Scott, E.M., Southon, J.R., Staff, R.A., Turney, C.S.M., Plicht, J.V.D., 2013. IntCal13 and Marine13 Radiocarbon Age Calibration Curves 0–50,000 Years cal BP. Radiocarbon 55, 1869–1887. doi:10.2458/azu_js_rc.55.16947

Reimer, P.J., Reimer, R.W., 2001. A Marine Reservoir Correction Database and On-Line Interface. Radiocarbon 43, 461–463. doi:10.1017/s0033822200038339

Schweinsberg, A.D., Briner, J.P., Miller, G.H., Bennike, O., Thomas, E.K., 2017. Local glaciation in West Greenland linked to North Atlantic Ocean circulation during the Holocene. Geology 45, 195–198. doi:10.1130/g38114.1

Schweinsberg, A.D., Briner, J.P., Miller, G.H., Lifton, N.A., Bennike, O., Graham, B.L., 2018. Holocene mountain glacier history in the Sukkertoppen Iskappe area, southwest Greenland. Quaternary Science Reviews 197, 142–161. doi:10.1016/j.quascirev.2018.06.014

Schweinsberg, A.D., Briner, J.P., Licciardi, J.M., Bennike, O., Lifton, N.A., Graham, B.L., Young, N.E., Schaefer, J.M., Zimmerman, S.H., 2019. Multiple independent records of local glacier variability on Nuussuaq, West Greenland, during the Holocene. Quaternary Science Reviews 215, 253–271. doi:10.1016/j.quascirev.2019.05.007

Thomas, E.K., Briner, J.P., Ryan-Henry, J.J., Huang, Y., 2016. A major increase in winter snowfall during the middle Holocene on western Greenland caused by reduced sea ice in Baffin Bay and the Labrador Sea. Geophysical Research Letters 43, 5302–5308. doi:10.1002/2016gl068513

Thomas, E.K., Castañeda, I.S., Mckay, N.P., Briner, J.P., Salacup, J.M., Nguyen, K.Q., Schweinsberg, A.D., 2018. A Wetter Arctic Coincident With Hemispheric Warming 8,000 Years Ago. Geophysical Research Letters 45. doi:10.1029/2018gl079517

van der Bilt, W.G., Rea, B., Spagnolo, M., Roerdink, D.L., Jørgensen, S.L., Bakke, J., 2018. Novel sedimentological fingerprints link shifting depositional processes to Holocene climate transitions in East Greenland. Global and Planetary Change 164, 52–64. doi:10.1016/j.gloplacha.2018.03.007

van der Bilt, W.G., Born, A., Haaga, K.A., 2019. Was Common Era glacier expansion in the Arctic Atlantic region triggered by unforced atmospheric cooling? Quaternary Science Reviews 222, 105860. doi:10.1016/j.quascirev.2019.07.042

Wagner, B., Bennike, O., 2012. Chronology of the last deglaciation and Holocene environmental changes in the Sisimiut area, SW Greenland based on lacustrine records. Boreas 41, 481–493. doi:10.1111/j.1502-3885.2011.00245.x

Weidick, A. 1976. 'Report of Activities, 1975', Gronlands Geologiske Undersogelse, 80, 136-144.

Winsor, K., Carlson, A.E., Welke, B.M., Reilly, B., 2015. Early deglacial onset of southwestern Greenland ice-sheet retreat on the continental shelf. Quaternary Science Reviews 128, 117–126. doi:10.1016/j.quascirev.2015.10.008

Woodroffe, S.A., Long, A.J., Lecavalier, B.S., Milne, G.A., Bryant, C.L., 2014. Using relative sea-level data to constrain the deglacial and Holocene history of southern Greenland. Quaternary Science Reviews 92, 345–356. doi:10.1016/j.quascirev.2013.09.008